PFC/JA-95-35

Papers Presented at the 22nd EPS Conference on Controlled Fusion and Plasma Physics by the Alcator C-Mod Group

(Bournemouth, England July 3-7, 1995)

Plasma Fusion Center
Massachusetts Institute of Technology
Cambridge, MA 02139

July 1995

This work was supported by the U. S. Department of Energy Contract No. DE-AC02-78ET51013.

Papers Presented at the 22nd EPS Conference
on Controlled Fusion and Plasma Physics by the Alcator C–Mod Group

Table of Contents

---

† Associazione EURATOM-ENEA sulla Fusione, Centro Richerche Frascati, Italy.
‡‡ Institute for Plasma Research, University of Maryland, College Park, MD.
‡ Japan Atomic Energy Research Institute, Naka, Ibaraki, Japan.
# Princeton University Plasma Physics Laboratory, Princeton, NJ.
** Department of Physics, The Johns Hopkins University, Baltimore, MD.
†† General Atomics, San Diego, CA.

An Investigation of the Extent of Divertor Detachment in Alcator C-Mod

B. Lipschultz, J.A. Goetz, I.H. Hutchinson, B. LaBombard, G. M. McCracken, A. Niemszewski, J.L. Terry, S.M. Wolfe
Plasma Fusion Center, Massachusetts Institute of Technology, Cambridge Ma. 02139 U.S.A.

Introduction

Understanding divertor detachment is essential to predicting the operation of future diverted tokamaks. The current plan for ITER operation assumes that the plasma is detached from the divertor, that $\bar{n}_e$ be near the Greenwald limit [1] and that the main plasma is not diluted by impurities. However, we do not know whether these conditions can be achieved simultaneously. In this set of experiments the core plasma parameters have been varied systematically in order to determine when divertor detachment starts, how the radial extent of detachment grows and how the detachment process can be controlled. Various divertor geometries have been studied in Alcator C-Mod, with most emphasis on equilibria with strike points on the vertical plates[2,3] as shown in Figure 1.

In general, the threshold density for divertor detachment of Alcator C-Mod plasmas has been found to be linearly dependent on the input power for ohmic plasmas [4]. T_e at the divertor plate is ~ 5 eV for flux surfaces about to detach. Under ohmic conditions the core density at the divertor detachment threshold is $\bar{n}_e \sim 0.25 \times n_{Greenwald}$. Other tokamaks, with more open, flat-plate divertor geometries, more typically find that the detachment threshold is closer to the Greenwald density limit (0.5-0.9 x $n_{Greenwald}$)[5]. More detailed characteristics of divertor detachment and the available diagnostics are found elsewhere [2,4,6].

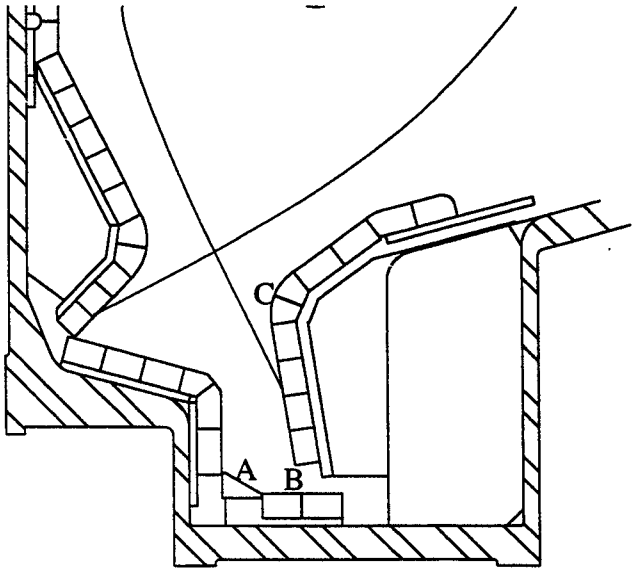

Figure 1: The Alcator C-Mod divertor configuration. A representative equilibrium with outer strike point on the vertical section of the plate is shown.

Density dependence of detachment

The detachment of plasma on a particular flux surface from the outer divertor plate has been determined by comparing the plasma pressure profiles at the target to upstream values in the SOL outside the divertor. Each flux surface is labeled by its distance outside the separatrix on the midplane (ρ in mm). The absolute uncertainty of this mapping is ± 1-2 mm but the relative uncertainty, shot to shot, is ~ 1 mm. Figure 2 shows the growth of the radial extent of detachment for typical ohmic 0.8 MA (5.3 Tesla) plasmas. Included are data from discharges with outer

divertor strike point on the vertical section (figure 1; region B-C) and with the strike point on the floor (figure 1; region A-B) - the so called 'slot-divertor' configuration. From this data it is clear that the radial extent of detachment is a strong function of $\bar{n}_e$ until the divertor pressure deficit reaches the 'nose' of the outer divertor (figure 1 point C). We have varied the density over the widest range for the vertical plate geometry and the detachment extent does not increase beyond the divertor nose even for densities 2.5 x the detachment threshold.

The effect of the divertor detachment on radiation in the divertor is similarly abrupt. Below the detachment threshold, divertor radiation is peaked near the inner and outer plate surfaces and the magnitude of the radiative loss increases with density. As the detachment of flux surfaces extends up the divertor face to the nose, the majority of the radiation in the divertor region moves inside the separatrix to just above the x-point. The emission distribution does not change as the density is increased further.

The detachment process can cause very large drops in pressure at the divertor surface. Figure 3a illustrates the density dependence of pressure ($2n_eT_e$) at different locations along the vertical plate for the discharges shown in figure 2. The pressure loss at the plate in the private flux region and at the separatrix is very large. Moving further out in the SOL, the effect of detachment on the plate pressure is gradually reduced up to the divertor nose (ρ = 6 mm). In the regions of the outer divertor plate beyond the nose the pressure increases with density, independent of the detachment. There may be some variation among the flux surfaces in the rate of pressure

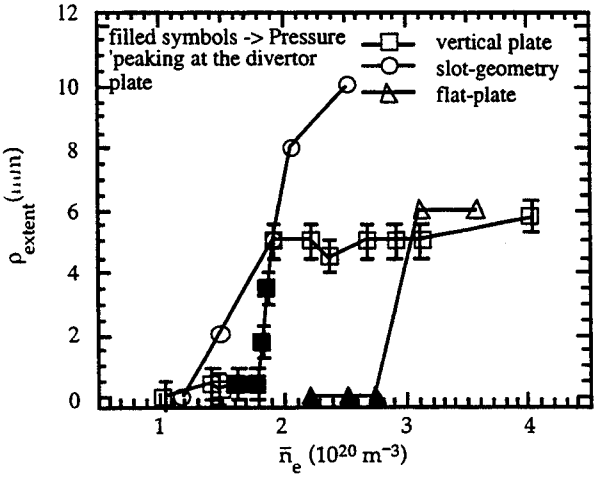

Figure 2: Extent of detachment at the outer divertor for 3 different geometries. ρ corresponds to the midplane radius of the detachment front.

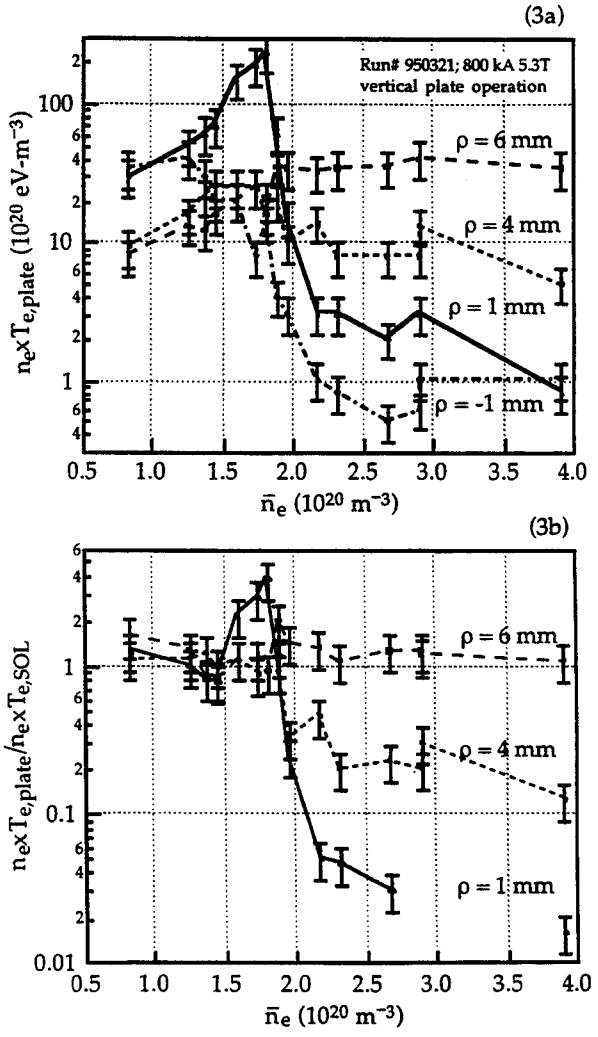

Figure 3: Effect of Detachment on outer divertor plate plasma pressure for vertical plate 800 kA ohmic case of figure 2: a) Plate pressure at different radii; b) Plate pressure normalized to corresponding SOL value.

loss with respect to $\bar{n}_e$ (e.g. the pressure at $\rho = 4$ mm drops more slowly than in the separatrix and private flux regions).

The pressure loss at the divertor surface can also be viewed as a pressure deficit with respect to the SOL outside the divertor. Figure 3b replots the data of 3a normalized to the pressure upstream on the same flux surface. The level of pressure deficit in the divertor ($2n_eT_{e,plate}/2n_eT_{e,SOL}$) is not necessarily a simple function of density. Often, a small pressure enhancement or `densified' region' (ρ = 1 mm curve) can appear before detachment spreads across the vertical section. The 'radial' width of this region is small (ρ = 1-2 mm).

Dependence of detachment threshold on divertor geometry

Some aspects of the Alcator C-Mod divertor geometry appear to have a strong effect on the characteristics of divertor detachment. As discussed above, the differences between vertical plate and slot operation are minimal in the onset of detachment. Another common feature is that the extent of detachment is limited to below the divertor nose; $\rho = 6$ mm for the vertical plate data shown and $\rho = 10$ mm for the slot geometry data. For all strike point locations in the region B-C of figure 1, the detachment density threshold does not vary, nor the observation of the localized pressure enhancement prior to detachment. As the strike point is moved closer to the divertor nose (location C) from below, the 'fraction' of the flux surfaces detached from the divertor surface and the fractional pressure loss are reduced.

In an effort to compare C-Mod results with divertor detachment characteristics in other devices a third mode of divertor operation was developed. The plasma is raised such that the inner and outer strike points are located above the divertor noses. Then the angle of separatrix intersection with the divertor plate and access of recycling neutrals to the SOL and core plasmas is similar to the more open, flat-plate divertor geometry found in other tokamaks. Field line lengths in the region below the x-point are decreased. Several differences emerge from this study: The $\bar{n}_e$ required for divertor detachment is increased by 50-80% above that found for equivalent (core conditions- input power, plasma current,...) vertical plate operation (see fig. 2); the pressure deficit at the plate is much smaller ($2n_eT_{e,plate}/2n_eT_{e,SOL} \sim 0.1$ compared to .01 for vertical plate). The extent of detachment increases as the density is increased with the initial pressure loss occurring at ρ =2 mm. The occurrence of a pressure enhancement before detachment initiates is also still observed for the flat-plate configuration.

Modification of the detachment threshold

Core parameters other than density can have a significant effect on the divertor detachment threshold. P_{SOL} (the power flowing across the separatrix), Ip and $B_{Toroidal}$ have all been varied as part of this study. It appears that the density threshold for detachment increases with P_{SOL} and decreases with increasing q. The strongest dependence is on q. Further experiments need to be carried out to test these preliminary results.

We have also studied the efficacy of lowering the detachment threshold by injecting neon gas. The detachment threshold has been reduced to ~ 60% of the non-neon value. Following divertor

detachment, impurity screening of impurities from the core plasma degrades[4,7], increasing both puffed and intrinsic impurities levels there. In these neon puffing experiments Z_{eff} rose from 1.2 to 1.8.

Summary

We find with vertical divertor plate operation that the radial extent of detachment increases strongly with increasing density until the detachment process reaches the 'nose' of the outer divertor, outside which the divertor plate is more horizontal. The detachment extent does not increase beyond the divertor nose even when the core density is more than doubled. Without auxiliary heating or addition of impurity gases, the detachment onset corresponds to $\bar{n}_e \sim 0.25$ x $n_{Greenwald}$. The detachment threshold increases with P_{SOL}, 1/q and moving the outer strike point above the divertor nose. It can be reduced through the addition of neon.

Discussion

The divertor nose plays an important role in limiting detachment (vertical plate geometry) and affecting the detachment threshold. One possible reason is that neutrals which recycle from regions of the divertor plate below the nose can repetitively travel back and forth between the private flux zone and the plate, each time participating in momentum loss processes. Neutrals originating from the divertor surface above the divertor nose are likely to travel to other regions (core, midplane or private flux vacuum regions) thus not repetitively removing ion momentum.

The q dependence of the detachment threshold can possibly be explained in terms of increased radiating volume with longer field line length in the divertor. The increased losses (along a flux surface) will reduce $T_{e,plate} \sim 5$ eV and bring on detachment. Increased P_{SOL} has the opposite effect.

Acknowledgements

The authors would like to thank the Alcator group for their assistance in acquiring this data and achieving the needed equilibria. This work is sponsored by the U.S. Department of Energy under contract No. DE-AC02-78ET51013.

References

[1] Greenwald, M., Terry, J.L., Wolfe, S.M., Ejima, S. et al, *Nucl. Fusion* **25** (1988).

[2] Hutchinson, I.H. et al, *Physics of Plasmas.* **1** 1511 (1994).

[3] LaBombard B., Lipschultz, B., Kochan, S. *Proceedings of the 14th IEEE/NPSS Symposium on Fusion Engineering* p 40, (1991).

[4] Lipschultz, B., Goetz, J.A., LaBombard, B., McCracken, G.M., Terry, J.L. et al, *J. Nucl. Materials* **220-222** 50 (1995)

[5] ITER divertor experts meeting Garching Germany, February 1995.

[6] LaBombard, B *Physics of Plasmas* **2** 2242 (1995)

[7] McCracken G.M. et al, *J. Nucl. Materials* **220-222** 164 (1995)

Impurity screening in Alcator C-Mod

G M McCracken, B Lipschultz, B LaBombard, F Bombarda*, M Graf,
J A Goetz, R Granetz, D Jablonski, H Ohkawa, J E Rice,
J L Terry , Y Wang and B L Welch.
Plasma Fusion Center
Massachusetts Institute of Technology
Cambridge, MA 02139
*Associazione EURATOM-ENEA sulla Fusione, Frascati, 00044,Italy

1. Introduction

One of the principal roles of the divertor is to prevent impurities produced at the target from returning to the confined plasma. A series of experiments has been carried out to investigate the screening effect of the divertor and SOL by injecting recycling (Ne and Ar) and non-recycling (CH_4 and N_2) gases at different locations in Alcator C-Mod diverted discharges. The use of gaseous impurities has the advantage of giving independent control of the injection rate under a range of operating conditions compared with studying intrinsic impurities. Spectroscopic measurements of impurity densities and detailed profiles of the plasma density and temperature in the divertor have been made.

2. Experiment.

Alcator C-Mod is a high field , high density, divertor tokamak [1,2]. Typical operating conditions for the present experiments are I_p=0.8 MA, $\bar{n}_e$=1.3-2.8x10^{20} m^{-3}, B_T=5 Tesla, $T_e(0)$=1.0-1.8 keV and elongation =1.6, in a single null diverted configuration. The arrangement of the impurity injection systems and the diagnostics is shown in fig 1. One gas injection system consists of an array of capillary tubes connected to poloidal positions, A and C, at the divertor target plates and the inner wall. A second system delivers gas to a point, B, near the outer midplane. The second system has a valve close to the vacuum vessel and is faster acting than the capillary system. Pulses of gas ~ 30 ms can be injected and the subsequent distribution of the impurities followed in space and time.[3]

The impurity radiation in the core plasma is measured with a single spatial channel, absolutely calibrated, VUV spectrograph and, in the case of the argon, also with a crystal spectrometer [4] viewing Ar XVII at up to 5 chords simultaneously. The impurity brightness in the divertor is monitored with a visible spectrometer using a 2-D CCD detector. A wavelength range of up to 45 (70) nm can be scanned in 30 ms with a spectral resolution of 0.1 (0.15) nm. Optical fibers view up to 14 locations at both the inner divertor, P,Q, and outer divertor, R,Q,

simultaneously, Fig 1. In addition there are core measurements of the n_e, T_e, total radiation and Z_{eff} profiles and other spectroscopic measurements. The n_e and T_e profiles in the SOL and along the target plates are measured with a scanning probe and an array of Langmuir probes in the tiles [5]. Typical conditions at the divertor plate which have been used for impurity injection experiments, vary from T_e=20 eV, n_e=1x10^{19} m^{-3} to T_e< 5 eV, n_e=3x$10^{20}m^{-3}$.

3. Results

With a short pulse (~40 ms) of neon or argon, typically 1 to 3% of the injected atoms get into the confined plasma and stay there for the duration of the discharge, Fig 2. The MIST code [6] is used to calculate the charge state distribution and hence the total impurity content, calibrating the results to the measured brightness of the Ar XVII or Ne VIII. The fraction of injected impurities entering the confined plasma decreases with density [3]. Gas has also been injected via the capillary tubes into the private flux zone in the divertor , at the inner wall midplane and into the outer SOL. If the impurity flow rate into the divertor is constant, (typically 1x10^{19} s^{-1}), the impurity density in the plasma increases roughly linearly during the length of the diverted phase. These results indicate that neon and argon are recycling impurities, as expected. The fraction getting into the core plasma does not depend strongly on the position of injection .

In the case of a pulse of nitrogen or methane the impurity concentration in the confined plasma decays with a time constant of ~ 30 ms after the injection pulse, Fig 3. This contrasts with the recycling gases. The time constant is comparable to that measured for impurities injected by laser ablation and indicates an impurity recycling coefficient $\leq$ 0.3. For a long impurity injection pulse the impurity concentration rises to a constant value. The impurity injection rate, obtained from the pressure rise in the vacuum vessel during a calibration pulse, has also been plotted in fig 3. It is observed that the total number of impurities in the plasma is proportional to the *injection rate* over the whole injection cycle, rather than the integrated amount as is the case for the recycling impurities. The total number of impurities in the core plasma can therefore be normalized to a constant influx for a range of different conditions. The results for nitrogen and carbon are shown in fig 4. The impurity number/influx is a time constant which varies from 10^{-5} to 10^{-2} s, depending on species and plasma conditions. Lower impurity core densities are obtained for carbon than for nitrogen and the number of core impurities decreases with increasing core electron density.

Using the measured SOL profiles of n_e and T_e, the ionization rate of both CH_4 and N_2 has been calculated as a function of minor radius. For typical C-Mod conditions the methane is ionized further from the separatrix than the nitrogen. This is consistent with a model in which the ionization occurs in the SOL and the impurity density in the confined plasma is determined by the dynamic flux balance between the injection rate, cross field diffusion to the separatrix and parallel flow in the SOL to the target. Direct observations of the parallel flow towards the divertor have been made by viewing the CII and CIII spatial distribution during CH_4 injection, using CCD

cameras and interference filters.

A background nitrogen impurity density is observed which builds up in successive discharges, indicating that nitrogen is accumulating on surfaces, probably the divertor target plates. In the case of carbon there is always significant background both for low and high charge states since carbon is an intrinsic impurity in C-Mod.

A preliminary assessment of the spatial distribution of the impurities in the divertor has been carried out using the multi-channel visible spectrograph with chords spanning the inner and outer divertor. In the case of argon the chordal brightness of Ar II is highest at the inner divertor. This is consistent with the measurements of the $D\alpha$ and the total radiation. At low to medium density the radiation comes from the region just above the inner divertor nose. The results are also consistent with probe measurements which show the temperature is much lower at the inner than the outer divertor target [5]. In the case of N and C there is little increase observed in the divertor radiation during impurity injection

4. Conclusions

There is a striking difference between the rare gases, Ne and Ar, and the non recycling species, C and N. In both cases there is good screening; this is attributed to the high plasma and power density which leads to high ionization rates in the SOL. The radial location of ionization is, in all cases, in the SOL. This is partly due to the low energy of the injected gas species. Less good screening is observed for laser injected scandium which has a directed energy ~10 eV. For sputtered atoms, with energies $\geq$ 5eV, the peak in the ionization is calculated to be much closer to the separatrix, also implying lower screening. The lower screening of sputtered atoms may account for the high carbon background and the buildup of the nitrogen background. In the case of non-recycling gas injection the effective loss time along the SOL is short compared to impurity transport times in the main plasma. It appears that most of the impurity flux is ionized in the SOL, then flows to the target and sticks there.

Acknowledgements: The authors are grateful to the whole Alcator team and in particular to the operations group, for the excellent operation of the machine. This work is sponsored by the US Department of Energy under contract No DE-AC02-78ET51013

References:

[1] I H Hutchinson, Physics of Plasmas, **1** 1511 (1994).
[2] B Lipschultz, J Goetz, B Labombard et al, J. Nucl. Mater., **220-222** 50 (1995).
[3] G M McCracken, F Bombarda, M Graf et al J. Nucl. Mater. **220-222** 264 (1995).
[4] J E Rice and E S Marmar, Rev Sci Instrum., **61** 2753 (1990)
[5] B Labombard, Phys of Plasmas,**2**, 2242, (1995)
[6] R A Hulse, Nuclear Technology/Fusion, **3** 259 (1983)

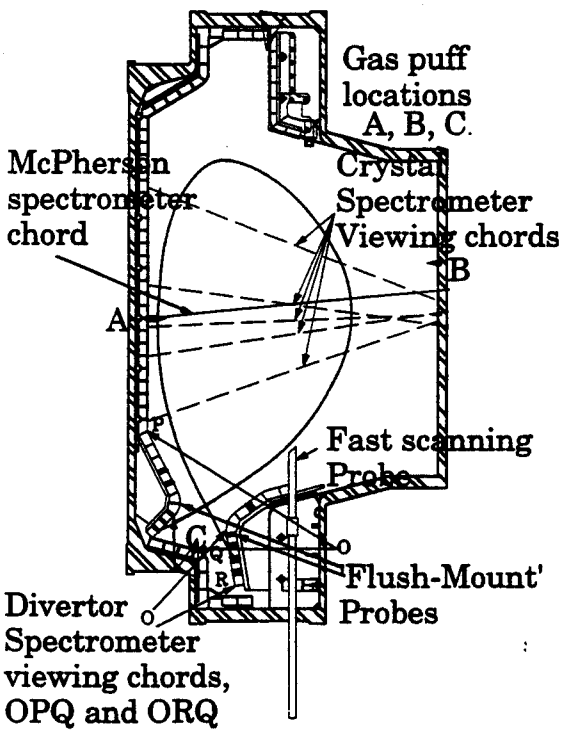

Fig 1. Poloidal cross section of C-Mod showing gas puffing positions and spectroscopic views

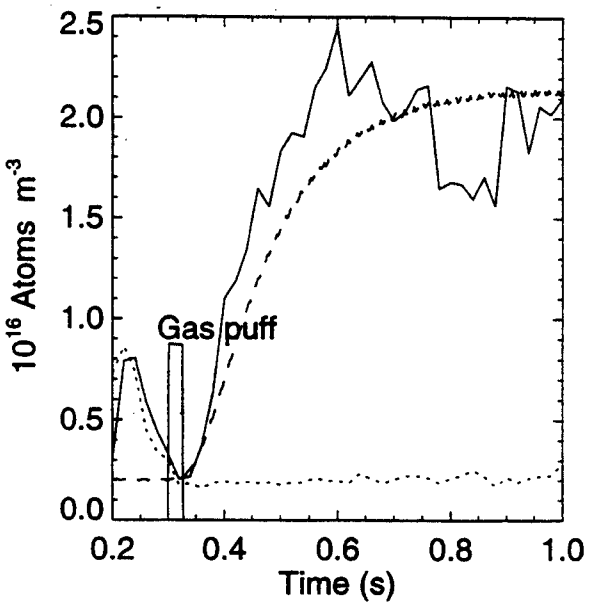

Fig 2. Argon atoms in the plasma with 30 ms gas puff, $\bar{n}_e = 1.6 \times 10^{20}$ m^{-3}

——— Ar in confined plasma

..... Ar background, no gas puff

- - - - - - - Ar atoms injectedx0.02

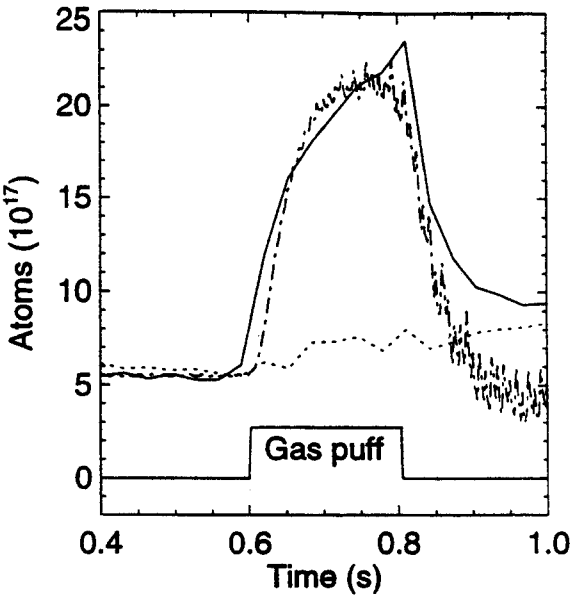

Fig 3. Nitrogen atoms in the plasma with 200 ms gas puff, $\bar{n}_e = 1.6 \times 10^{20}$ m^{-3}

——— N in confined plasma

..... N background, no gas puff

- - - - - - - N *injection rate* x0.005/s

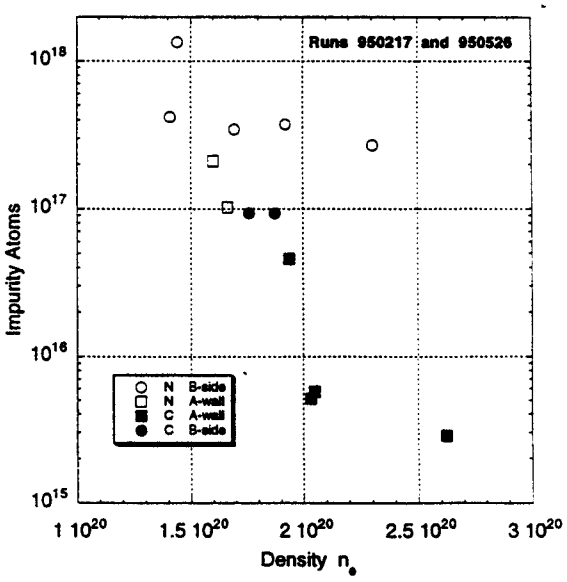

Fig 4. N and C atoms in the plasma for an injection rate of 1×10^{20}/s at inner wall, A and outer midplane, B

ICRF Heating and Enhanced Confinement Modes in Alcator C-Mod*

Y. Takase, R. Boivin, F. Bombarda,† P. Bonoli, C. Fiore, D. Garnier, J. Goetz, S. Golovato, M. Graf, R. Granetz, M. Greenwald, S. Horne, A. Hubbard, I. Hutchinson, J. Irby, H. Kimura,‡ B. LaBombard, B. Lipschultz, R. Majeski,# E. Marmar, M. May,** A. Mazurenko, G. McCracken, A. Niemczewski, P. O'Shea, R. Pinsker,†† M. Porkolab, J. Reardon, J. Rice, C. Rost, J. Snipes, J. Terry, R. Watterson, B. Welch,‡‡ S. Wolfe

MIT Plasma Fusion Center, Cambridge, MA 02139 U.S.A.

1. Introduction

Alcator C-Mod ($R = 0.67\,\mathrm{m}$, $a = 0.22\,\mathrm{m}$, $\kappa = 1.7$ typical) is a compact high field tokamak with all metallic (mostly molybdenum) plasma facing components. Presently, two transmitters at a frequency of 80 MHz, each capable of 2 MW output, are operational. C-Mod has operated successfully up to a toroidal field of 8.0 T and a plasma current of 1.2 MA, and up to 3.5 MW of RF power has been coupled into the plasma using two dipole antennas (two current straps driven out of phase). The main heating scenario employed thus far has been H minority heating in D majority plasmas at 5.3 T. Other scenarios investigated include ^{3}He minority heating in D majority at 8.0 T, second harmonic H minority heating in D majority at 2.6 T, and mode conversion electron heating in H-^{3}He plasmas at 6.5 T. Second harmonic ^{3}He minority heating in D majority plasmas at 4.0 T was not successful. H-mode is routinely observed, and P-mode is observed in combination with lithium pellet injection.

2. L-Mode

D(H) heating of L-mode plasmas was performed in the parameter range $B_T(0) = 3.5 - 5.5\,\mathrm{T}$, $I_p = 0.4 - 1.2\,\mathrm{MA}$, $\overline{n}_e = (0.5 - 3) \times 10^{20}\,\mathrm{m}^{-3}$ (target), and $n_H/n_{H+D} = 0.01 - 0.2$. At high RF powers it was necessary to reverse the direction of the ion ∇B drift direction (away from the X-point) to prevent the plasma from going into H-mode.

Central temperatures of $T_{e0} = 5.8\,\mathrm{keV}$ (top of sawtooth) and $T_{i0} = 4.0\,\mathrm{keV}$ (sawtooth averaged) were obtained at $\overline{n}_e = 1 \times 10^{20}\,\mathrm{m}^{-3}$ with $P_{RF} = 3.5\,\mathrm{MW}$. Heating is most effective at low H concentrations ($n_H/n_e < 0.05$). Degradation of heating at

* Supported by U.S. D.O.E. Contract No. DE-AC02-78ET51013.

† Associazione EURATOM-ENEA sulla Fusione, Frascati 00044 Italy

‡ Japan Atomic Energy Research Institute, Naka, Ibaraki, Japan

\# Princeton University Plasma Physics Laboratory, Princeton, NJ, U.S.A.

** Department of Physics, The John Hopkins University, Baltimore, MD, U.S.A.

†† General Atomics, San Diego, CA, U.S.A.

‡‡ Institute for Plasma Research, University of Maryland, College Park, MD, U.S.A.

higher H concentrations is more pronounced at higher electron densities. Heating degrades gradually as the resonance layer is moved off-axis by reducing the toroidal field, with no heating observed when the resonance layer is moved out to $r/a \geq 0.75$.

For on-axis D(H) heating the absorption efficiency, estimated from the discontinuity of slope in the diamagnetic stored energy, was very high (80–100%). The plasma current and input power dependences of energy confinement are roughly consistent with the ITER89-P scaling, as shown in Fig. 1. However, there is an indication of gradual degradation of confinement at higher densities, as well as at very low densities ($\overline{n}_e < 1 \times 10^{20}\,\mathrm{m}^{-3}$).

3. H-Mode

ICRF heated H-mode is routinely observed in C-Mod. Almost all high power ($\gtrsim 2\,\mathrm{MW}$) RF heated discharges make the transition into H-mode, even with the outer gap (separatrix to outboard limiter distance) as small as 1 cm. No special wall conditioning is required to obtain the H-mode.

The H-mode power threshold (with the ion ∇B drift directed toward the lower single-null X-point) scales similarly to the ITER scaling $P/S(\mathrm{MW/m^2}) = 0.044\,\overline{n}_e B_T$ ($10^{20}\,\mathrm{m}^{-3}\,\mathrm{T}$) [1], but H-mode transitions well below this threshold (by up to a factor of 2) are often observed, as shown in Fig. 2. The peaked density profile after Li pellet injection seems to be beneficial for accessing the H-mode. We note here that the values of P/S and $\overline{n}_e B_T$ achieved in C-Mod are an order of magnitude greater than those achieved in ASDEX-UG, DIII-D, and JET, and are comparable to or greater than what is expected for ITER. H-mode was not observed when the ion ∇B drift was away from the X-point, indicating that the H-mode power threshold in this case is higher by at least a factor of 2. H-mode was observed up to a target density of $\overline{n}_e = 2.6 \times 10^{20}\,\mathrm{m}^{-3}$ ($\overline{n}_e = 3.2 \times 10^{20}\,\mathrm{m}^{-3}$ during the density decay after Li pellet injection). However, H-mode has not been observed below a low density limit of $\overline{n}_e \simeq 1 \times 10^{20}\,\mathrm{m}^{-3}$.

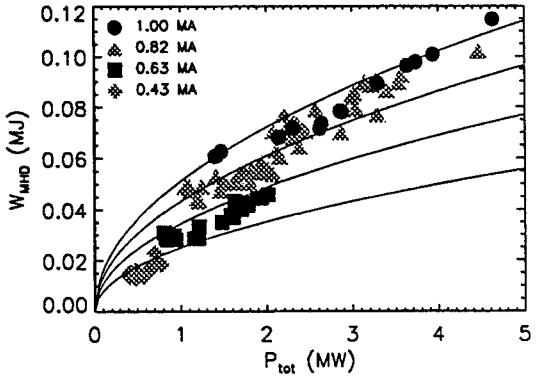

Fig. 1: L-mode confinement. Solid lines represent the ITER89-P scaling.

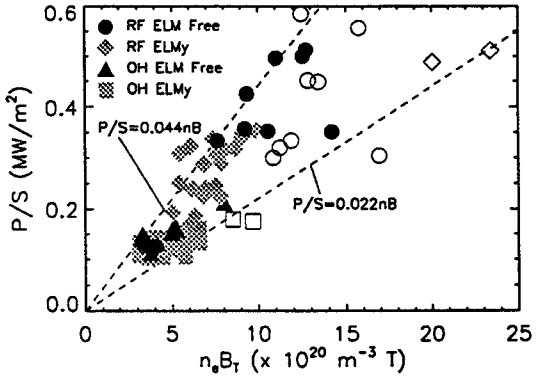

Fig. 2: H-mode threshold. Open symbols indicate plasmas with Li pellet injection.

An H-factor (energy confinement enhancement over the ITER89-P L-mode scaling

[2]) for ICRF heated ELM-free H-modes of up to 1.5 has been observed. For our parameters, ITER94 ELM-free H-mode scaling [3] predicts 1.6 – 1.8 for the H-factor. In ohmic ELM-free H-modes at $B_T = 3.5\,\mathrm{T}$, H-factors of up to 2 have been observed [4].

4. P-Mode (PEP Mode)

Li pellet (1.2×10^{20} electrons) injection followed by central ICRF heating produces the PEP mode [5]. These plasmas are characterized by highly peaked density and ion temperature profiles, resulting in an enhanced fusion rate, typically by an order of magnitude over similar L-mode discharges. The PEP mode is observed over a wide range of target densities ($\overline{n}_e = 1.0 - 2.5 \times 10^{20}\,\mathrm{m}^{-3}$), but only when the pellet penetrates to the plasma center.

In the 7.9 T, 1 MA discharge (^{3}He minority heating) shown in Fig. 3 a fusion neutron rate of $9 \times 10^{13}\,\mathrm{sec}^{-1}$, $T_{i0} = 3.7\,\mathrm{keV}$, and $T_{e0} = 3.0\,\mathrm{keV}$ were obtained at $\overline{n}_e = 2.9 \times 10^{20}\,\mathrm{m}^{-3}$ with $P_{RF} = 2.5\,\mathrm{MW}$. In this example a transition into ELMy H-mode occurred at 0.828 sec and a transition into ELM-free H-mode occurred at 0.845 sec, but the neutron rate starts to decline after 0.830 sec. Simultaneous PEP and H-modes have also been observed. The cause of PEP mode termination is not well understood. It is sometimes, but not always, accompanied by enhanced MHD activity. It appears to be related to the loss of the peaked density profile. The neutron rate starts to decline when the density peak-to-average ratio $n_{e0}/\overline{n}_e$ falls below a critical level of approximately 1.5.

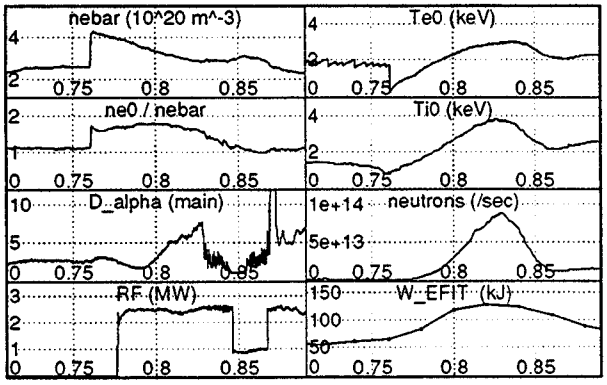

Fig. 3: D(^{3}He) PEP mode at $B_T = 7.9\,\mathrm{T}$ and $I_p = 1\,\mathrm{MA}$.

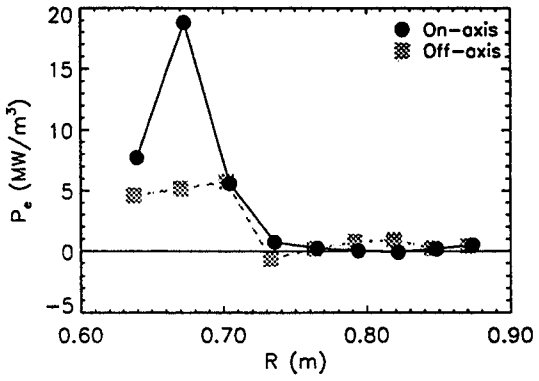

Fig. 4: Power deposition profiles for on-axis and off-axis mode conversion electron heating.

5. Mode Conversion Electron Heating

Highly localized direct electron heating using the mode converted ion Bernstein wave (IBW) [6] was observed in H-^{3}He plasmas at 6.5 T. H-^{3}He plasmas are analogous to D-T plasmas, because $\Omega_H/\Omega_{^3He} = \Omega_D/\Omega_T$. At this field, the H resonance is at $R = 0.82\,\mathrm{m}$ and the ^{3}He resonance is at $R = 0.55\,\mathrm{m}$, both more than half way out radially from the plasma center. Mode conversion to IBW occurs near the ion-ion hybrid layer, which shifts toward the high field side as the ^{3}He concentration is decreased or

the toroidal field is reduced. The IBW is strongly damped near the mode conversion layer. Effective central electron heating is observed with $n_{^3He}/n_e \simeq 0.25$ when the mode conversion occurs near the plasma center.

An electron heating power density (determined from the sawtooth reheat rate) of $25\,\mathrm{MW/m^3}$ was obtained with $P_{RF} = 1.4\,\mathrm{MW}$, an order of magnitude larger than the ohmic value with $P_{OH} = 1.1\,\mathrm{MW}$. The central electron temperature increased to 5.1 keV from an ohmic value of 2.3 keV [7]. The RF power deposition profile can be determined from the break of slope of the electron temperature at RF power steps. When the power deposition is inside the sawtooth inversion radius the RF power deposition can be determined from the difference in the sawtooth reheat rate between RF heated and ohmic phases. When both measurements are available, the two methods yield the same result. The RF power deposition profiles for on-axis and (near center) off-axis heating are shown in Fig. 4. For on-axis heating, the heating profile was highly peaked with a FWHM of 5 cm, compared to a typical FWHM of 13 cm for H minority heating.

6. CONCLUSIONS

Efficient ICRF heating of high density ($\overline{n}_e \lesssim 3 \times 10^{20}\,\mathrm{m^{-3}}$) plasmas was obtained in Alcator C-Mod at ITER relevant power densities ($P/S \lesssim 0.6\,\mathrm{MW/m^2}$). For on-axis D(H) heating at 5.3 T near complete absorption is achieved. The energy confinement in L-mode plasmas was found to be consistent with the ITER89-P scaling. Central temperatures of $T_{e0} = 5.8\,\mathrm{keV}$ (top of sawtooth) and $T_{i0} = 4.0\,\mathrm{keV}$ (sawtooth averaged) were obtained in an L-mode plasma at $\overline{n}_e = 1 \times 10^{20}\,\mathrm{m^{-3}}$. H-mode is routinely observed with ICRF heating. The highest stored energy of 130 kJ was achieved in an ELM-free H-mode plasma. The highest fusion reactivity of $9 \times 10^{13}\,\mathrm{sec^{-1}}$ was obtained in a PEP mode plasma with Li pellet injection and on-axis ICRF heating. At $B_T = 6.5\,\mathrm{T}$ highly localized direct electron heating by the mode converted IBW was observed in H-^{3}He plasmas. The near term plans call for the addition of 4 MW of tunable (40–80 MHz) power and a FWCD antenna in collaboration with PPPL.

REFERENCES

[1] F. Ryter, et al., Proc. 20th EPS Conf. on Cont. Fusion and Plasma Physics, 1993 (Lisboa), Vol. 17C, Part I, I-23.

[2] P.G. Yushmanov, et al., Nucl. Fusion **30**, 1999 (1990).

[3] K. Thomsen, et al., Nucl. Fusion **34**, 131 (1994).

[4] J. Snipes, et al., Nucl. Fusion **34**, 1039 (1994).

[5] B. Tubbing, et al., Nucl. Fusion **31**, 389 (1991).

[6] R. Majeski, et al., Phys. Rev. Lett. **73**, 2204 (1994).

[7] Y. Takase, et al., to be published in Radio Frequency Power in Plasmas (Proc. 11th Top. Conf., Palm Springs, CA, 1995), AIP, New York.